Progress in Oceanography 180 (2020) 102223

Contents lists available at ScienceDirect

Progress in Oceanography

journal homepage: www.elsevier.com/locate/pocean

Impact of physical and biological processes on temporal variations of the ocean carbon sink in the mid-latitude North Atlantic (2002–2016)

Vlad A. Macovei[a,b,*,1], Susan E. Hartman[a], Ute Schuster[c], Sinhué Torres-Valdés[d], C. Mark Moore[b], Richard J. Sanders[a,2]

[a] National Oceanography Centre Southampton, UK
[b] University of Southampton, UK
[c] University of Exeter, UK
[d] Alfred Wegener Institute, Germany

ARTICLE INFO

Keywords:
pCO_2 variability
CO_2 flux
Biological production
North Atlantic

ABSTRACT

The ocean is currently a significant net sink for anthropogenically remobilised CO_2, taking up around 24% of global emissions. Numerical models predict a diversity of responses of the ocean carbon sink to increased atmospheric concentrations in a warmer world. Here, we tested the hypothesis that increased atmospheric forcing is causing a change in the ocean carbon sink using a high frequency observational dataset derived from underway pCO_2 (carbon dioxide partial pressure) instruments on ships of opportunity (SOO) and a fixed-point mooring between 2002 and 2016. We calculated an average carbon flux of 0.013 Pg yr^{-1} into the ocean at the Porcupine Abyssal Plain (PAP) site, consistent with past estimates. In spite of the increase in atmospheric pCO_2, monthly average seawater pCO_2 did not show a statistically significant increasing trend, but a higher annual variability, likely due to the decreasing buffer capacity of the system. The increasing ΔpCO_2 led to an increasing trend in the estimated CO_2 flux into the ocean of 0.19 ± 0.03 mmol m^{-2} day^{-1} per year across the entire 15 year time series, making the study area a stronger carbon sink. Seawater pCO_2 variability is mostly influenced by temperature, alkalinity and dissolved inorganic carbon (DIC) changes, with 77% of the annual seawater pCO_2 changes explained by these terms. DIC is in turn influenced by gas exchange and biological production. In an average year, the DIC drawdown by biological production, as determined from nitrate uptake, was higher than the DIC increase due to atmospheric CO_2 dissolution into the surface ocean. This effect was enhanced in years with high nutrient input or shallow mixed layers. Using the rate of change of DIC and nitrate, we observed Redfieldian carbon consumption during the spring bloom at a C:N ratio of 6.2 ± 1.6. A comparison between SOO and PAP sustained observatory data revealed a strong agreement for pCO_2 and DIC. This work demonstrates that the study area has continued to absorb atmospheric CO_2 in recent years with this sink enhancing over time. Furthermore, the change in pCO_2 per unit nitrate became larger as surface buffer capacity changed.

1. Introduction

The cumulate emissions of carbon by human activities since the industrial revolution have caused atmospheric CO_2 concentrations to approach 410 ppm in 2018 (Le Quéré et al., 2018a), a number not seen on Earth for the past 3 million years (Seki et al., 2010). The atmospheric concentration would be even higher and climate change would proceed much faster had the ocean not taken up approximately a quarter of the cumulative anthropogenic carbon emitted between 1870 and 2016 (Le Quéré et al., 2018b). Although the global ocean is an overall carbon sink, the distribution of the sources/sinks varies across its surface (Takahashi et al., 2009). Of the sink regions, the North Atlantic is the largest per surface area, taking up a total of 0.7 ± 0.1 Pg C annually (Gruber et al., 2002). The size and evolution of the sink is a matter of considerable societal interest.

The ocean's ability to take up carbon from the atmosphere is determined by the Revelle factor, the ratio of change in carbon dioxide to the change in total DIC (Broecker et al., 1979; Egleston et al., 2010). Low Revelle factors correspond to high buffer capacity in regions such as the North Atlantic, and reflect an enhanced ability to absorb

* Corresponding author
E-mail address: vlad.macovei@hzg.de (V.A. Macovei).
[1] Currently at Helmholtz-Zentrum Geesthacht, Germany.
[2] Currently at Norwegian Research Centre, Bjerknes Centre for Climate Research, Norway.

https://doi.org/10.1016/j.pocean.2019.102223
Received 17 April 2019; Received in revised form 12 September 2019; Accepted 13 November 2019
Available online 20 November 2019
0079-6611/ © 2019 The Author(s). Published by Elsevier Ltd. This is an open access article under the CC BY license (http://creativecommons.org/licenses/BY/4.0/).

atmospheric CO_2 (Bates et al., 2014). The anthropogenic increase in atmospheric CO_2 and corresponding ocean uptake will drive an increase in oceanic pCO_2 and a consequential decrease in the oceanic buffer capacity (Iida et al., 2015; Sabine et al., 2004). In the modern ocean, the Revelle factor is increasing in response to carbon accumulation (Fassbender et al., 2017). In addition, absorption of CO_2 leads to a reduction in pH and lowering of calcium carbonate saturation state in the surface ocean. This process, known as ocean acidification, potentially leads to decreased calcification and growth rates in some calcifying species (Doney et al., 2009). At the moment, natural variability is masking some of the anthropogenic effect on ocean sinks (McKinley et al., 2016), but studies from Le Quéré et al. (2010) – for the 1981 to 2007 period or Schuster and Watson (2007) – for 1994 to 2005, showed that regionally, current sinks can become weaker. Long term studies found that between 1990 and 2006 (Schuster et al., 2009) and between 1993 and 2005 (McKinley et al., 2011), the mid and high-latitude North Atlantic seawater pCO_2 increased at faster rates than the atmospheric rate. In fact, due to the decrease in buffer capacity of the northern North Sea, the North Sea basin shifted from being an overall sink to an overall source of atmospheric CO_2 in 2011 (Clargo et al., 2015). Changes such as this one emphasise the importance of long-term observations of the surface ocean. The existing global network of fixed point ocean observatories has produced important time series of biogeochemical variables, but the effective footprints of these observatories are estimated to only reflect around 9–15% of the ocean surface (Henson et al., 2016). Ships of Opportunity (SOO) equipped with CO_2 measuring facilities are an additional way of monitoring by sampling different regions and having a large observational capacity. This is particularly important since better understanding of the role of oceans in the global carbon budget has been identified as a major challenge (Steinberg et al., 2001).

In this study we make use of observations of carbon and nutrients collected on a SOO route between 2002 and 2016 combined with ancillary modelled and observational oceanographic and atmospheric data to investigate (1) variability, (2) trends, and (3) physical and biological drivers of the mid-latitude North Atlantic Ocean carbonate system. The SOO route passes in the vicinity of the Porcupine Abyssal Plain sustained observatory (PAP-SO; 49° N, 16.5° W), an area where the variability of the carbon parameters has previously been studied (Hartman et al., 2015). This allows an inter-comparison to be performed. The PAP-SO is found within the NA-STSS biome (Fay and McKinley, 2014), where data-based methods suggested a relatively stable air-sea flux between 1990 and 2010 (Rödenbeck et al., 2015), but neural network methods found a decrease in the carbon sink between 1998 and 2007 (Landschützer et al., 2013). There are still significant uncertainties regarding the interannual to decadal variability of the ocean carbon sink in this region.

2. Materials and methods

2.1. Data acquisition and processing

The main source of data for this study derives from the analysis of water samples collected aboard commercial ships chartered by *Geest Line Ltd.* (Fareham, UK): MV *Santa Maria*, MV *Santa Lucia* and MV *Benguela Stream*. These ships transited between the UK and the Caribbean nearly every month over the study period (Hartman et al., 2010). An automated underway CO_2 system provides continuous measurements of surface seawater temperature (SST), salinity (SSS) and fCO_2 (carbon dioxide fugacity) – converted to pCO_2 (carbon dioxide partial pressure) (Pierrot et al., 2009). These data are available from the Surface Ocean CO_2 Atlas (SOCAT version 6, SOCAT flags A-E, WOCE flag 2; www.socat.info; Bakker et al., 2018). While SSS is not quality controlled in SOCAT, we are confident with the data. On the UK-Caribbean line, salinity bottle samples are collected regularly, analysed at the National Oceanography Centre, UK, and used to calibrate the

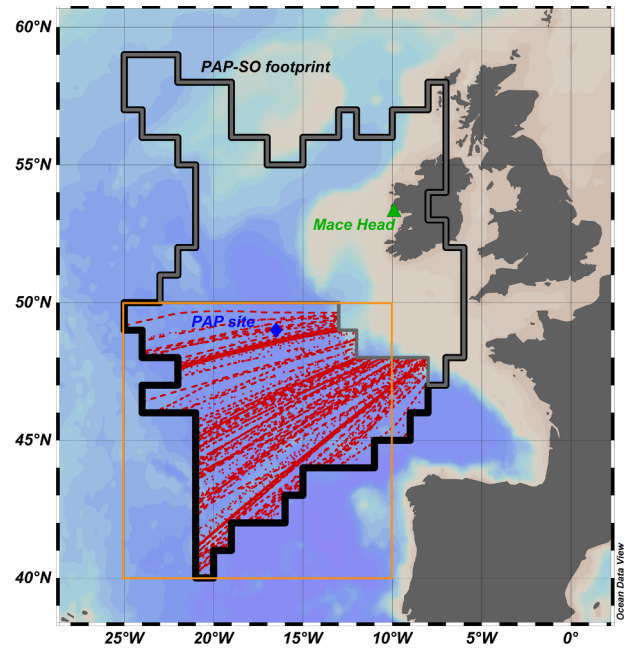

Fig. 1. Map of the study area showing all pCO_2 measurement locations in red symbols, the PAP footprint as the black contour, the excluded area as the grey contour, the location of the mooring at the PAP-SO site as the blue diamond and Mace Head atmospheric observatory as the green triangle. The orange box shows the extent of the NPP data selected. Produced with Ocean Data View (Schlitzer, 2016).

sensor. In addition, water samples were collected every 4 h in 15 mL plastic tubes and frozen immediately for later analysis of inorganic nutrients (nitrate + nitrite – hereby nitrate, silicate, phosphate) in the laboratory on shore. Nutrient data are available from the British Oceanographic Data Centre (doi: 10.5285/7a7b497a-c47b-0a69-e053-6c86abc07ef0). We selected data within the 'footprint' of the PAP-SO. This footprint was defined by Henson et al. (2016) as the spatial area where the outputs from Earth System Models have similar mean and variability to the station time series. We used the footprint that they calculated with pH as a parameter since this present study deals with the carbonate system and pH is the only carbonate system parameter considered in their study. Thus, we selected data within the boundaries of this area. In addition, we excluded from the analysis any measurements taken in the shelf areas to avoid the influence of coastal processes (Fig. 1). Our study area also lies within the North Atlantic Drift (NADR) biogeographic province as defined by Longhurst (2006). The SOO used in the present study have occupied this route since 2002, but other cruises were conducted in this area before, making it one of the most regularly observed ocean regions and allowing a long term assessment of change in the surface mid-latitude North Atlantic Ocean. Monthly averages were first prepared for all parameters and used in subsequent calculations. For months when surface pCO_2 data were not available on the usual route, the gaps were filled with values measured by other ships in the same area, also available from SOCAT. When nitrate measurements were not available for a particular month, the long-term climatological value (obtained from the results of this study) was used as a replacement. The same climatological gap-filling method was not used for pCO_2 since one of the objectives of this study was precisely to investigate interannual variability and differences from mean annual pCO_2.

Available SST and SSS data were used to estimate total alkalinity using the empirical equation derived by Lee et al. (2006) for the 30° N – 80° N North Atlantic region. We assume the empirical relationship between SSS and alkalinity is valid for the entire time series. With two of the carbonate system parameters now determined (pCO_2 and total

alkalinity), all others can be mathematically derived. We used the Matlab *CO2SYS* toolbox (Heuven et al., 2011) with the Lueker et al. (2000) K1 and K2 dissociation constants and the Dickson et al. (1990) K SO_4 constant to obtain dissolved inorganic carbon (DIC) concentrations. In order to eliminate potential freshwater influences, the DIC was normalised (nDIC) to the area average salinity (35.6).

Atmospheric xCO_2 (dry mole fraction) data were downloaded from the World Data Centre for Greenhouse Gases from the Mace Head station (WDCGG, 2018). This was chosen due to the proximity to our study area.

Monthly mean atmospheric pressure, dew point temperature and wind speed were obtained from the ERA-Interim (Dee et al., 2011), a reanalysis that combines model derived data and observations to produce a best estimate of global atmospheric and oceanographic parameters.

We used mixed layer depth (MLD) from Argo floats with data hosted by the Scripps Institution of Oceanography, UC San Diego and available every month of our time series (Holte et al., 2017), defined as the depth at which a density difference of 0.03 kg m^{-3} relative to the surface was found.

Since no measurements on the UK-Caribbean route were taken north of 50° N, we further restricted the area part of the PAP-SO footprint that was investigated in this study (Fig. 1). Extra SOCAT data and ancillary variables were only selected from this defined area.

Satellite-derived net primary productivity was downloaded from the Ocean Productivity website (Ocean Productivity, 2016) calculated according to Behrenfeld and Falkowski (1997). These data were selected from within the area shown in Fig. 1.

2.2. Calculations

The dry mole fraction of atmospheric CO_2 is converted to the partial pressure of atmospheric CO_2 by

$$pCO_2 = xCO_2(P_b - P_v)/1.01325 \tag{1}$$

(Humphreys et al., 2018), where P_b is the barometric pressure [bar] and P_v is the water vapour pressure [bar], calculated by

$$P_v = 610.94 \times \exp[(17.625T_{dp})/(243.04 + T_{dp})] \times 10^{-5} \tag{2}$$

where T_{dp} is the dew point temperature [°C] (Alduchov and Eskridge, 1996).

With both atmospheric and seawater pCO_2 known, sea-air CO_2 flux [mmol m^{-2} day^{-1}] was calculated following Wanninkhof (2014):

$$F = k\alpha(pCO_2^{sw} - pCO_2^{atm}) \tag{3}$$

where k is the gas transfer velocity [m day^{-1}] and α is the solubility of CO_2 [mmol m^{-3} atm^{-1}] (Weiss, 1974). The gas transfer velocity is calculated using the Schmidt number and the wind speed, while α is a function of SST and SSS. Negative values indicate flux from the atmosphere into the ocean (Wanninkhof et al., 2013). We calculated air-sea CO_2 fluxes using code freely available online (https://github.com/mvdh7/co2flux) – see Humphreys et al. (2018). Water density used for unit conversions was calculated using the Seawater Oceanographic Toolbox (McDougall and Barker, 2011).

With the information generated as above, the contributions of physical and biological processes to monthly changes in nDIC can be calculated. We used the same 'model' employed by Jiang et al. (2013). Firstly, we determined the gas exchange influence using

$$\Delta DIC_{Gas} = F/MLD_{(i)} \tag{4}$$

where ΔDIC_{Gas} is the gas exchange term, F is the sea-air CO_2 flux converted to μmol m^{-2} $month^{-1}$ and $MLD_{(i)}$ is the average mixed layer depth for that particular month. Then, we determined the biological production influence using

$$\Delta DIC_{BP} = (NO_{3(i)} - NO_{3(i-1)}) \times [(MLD_{(i)} + MLD_{(i-1)})/2] \times (C{:}\,N_{ratio})/MLD_{(i)} \tag{5}$$

where ΔDIC_{BP} is the biological production term, NO_3 is the average nitrate + nitrite concentration, 'i' is the month, $(MLD_{(i)} + MLD_{(i-1)})/2$ is the average mixed layer depth of two consecutive months and the $C{:}N_{ratio}$ is the carbon to nitrogen ratio of biological production/remineralization: 6.6 for this study (Frigstad et al., 2015; Henson et al., 2003).

When surface nitrate is replenished in winter, DIC is also brought up, but this mixing term is not given an individual decomposition term due to the high uncertainties.

The difference between the observed changes and the sum of the individual contributions gives a residual term, which includes vertical mixing.

$$\Delta DIC_{Residual} = \Delta DIC_{Observed} - \Delta DIC_{Gas} - \Delta DIC_{BP} \tag{6}$$

All the above mentioned changes in DIC have a corresponding effect on the seawater pCO_2. The $\Delta pCO_2(DIC_{Gas})$, $\Delta pCO_2(DIC_{BP})$ and $\Delta pCO_2(DIC_{Residual})$ were determined with the *CO2SYS* toolbox by forcing respective changes in the DIC input term. In addition, the $\Delta pCO_2(Alk)$ was calculated from changes in alkalinity, corrected for the changes in nitrate according to the nutrient H^+-compensation principle (Wolf-Gladrow et al., 2007). Unlike DIC, pCO_2 is also influenced by changes in SST. The temperature-induced change in seawater pCO_2 is calculated using the empirically determined thermodynamic relationship described by Takahashi et al. (2009):

$$\Delta pCO_2(Temp) = pCO_2(i-1) \times e^{0.0433\times(Temp(i)-Temp(i-1))-4.35\times10^{-5}[(Temp(i)^2-Temp(i-1)^2]} \tag{7}$$

where $Temp(i)$ and $Temp(i-1)$ are the mean SST of the current and previous months respectively.

As with DIC, the difference between the observed changes and the sum of the calculated components was assigned to a $\Delta pCO_2(Residual)$ term.

Finally, the individual monthly contributions to the carbonate system changes were combined to produce annual cycles. These show the relative importance of the different processes and also help assess the temporal variability within the PAP footprint when comparing to individual years.

2.3. Uncertainties

Given the multiple data sets used, with respective associated uncertainties and given the complex nature of the CO_2 toolboxes employed, we assess uncertainty of our calculations via a Monte Carlo simulation, similar to past studies (Fröb et al., 2018; Palevsky and Quay, 2017). We used the 6.4 μmol kg^{-1} uncertainty defined by Lee et al. (2006) for their North Atlantic alkalinity calculation and the 10 μatm error range for flags A-E in the SOCAT database (Lauvset et al., 2018). This is the largest uncertainty allowed in the database but a great majority of the measurements used were more accurate. The results of this simulation are therefore an upper-bound error estimation. We used a 0.1 μatm uncertainty for atmospheric pCO_2 measured at Mace Head (Derwent et al., 2002). Since most calculations in this study are performed using monthly averages, the SSS, SST and wind speed standard deviation of the monthly averages were used as their respective uncertainties. These uncertainty intervals are shown in Table 1.

A total of 1000 simulations were run with the input terms at each of 10 random locations using the *CO2SYS* toolbox to determine DIC and the *CO2flux* toolbox to determine CO_2 flux. The input parameters (Table 1) were allowed to vary randomly within the ± uncertainty interval. The DIC standard deviation as a percentage of the mean value of the simulations was found to vary between 0.27 and 0.30%. The CO_2

Table 1
Range of standard deviations as percentage of mean values for the output of the *CO2SYS* and *CO2flux* toolboxes obtained by running 1000 Monte Carlo simulations for 10 random locations.

Method used	% error	Input term	± error	Method used	% error
CO2SYS	**0.27-0.30**	Alkalinity	6.4 μmol kg^{-1}	CO2flux	**16-34**
		Salinity	0.26 PSU		
		Temperature	0.84 °C		
		Seawater pCO_2	10 μatm		
		Air pCO_2	0.1 μatm		
		Wind speed	0.82 m s^{-1}		

flux standard deviation as a percentage of the mean value of the simulations varied between 16 and 34%, with higher uncertainties for fluxes closer to 0. These large values are mainly driven by the large range in the wind speed estimations inside the PAP footprint. When all other input terms were kept fixed and only wind speed allowed to vary, the resulting error was of a similar range. The significant effect of the choice of wind product and the use of monthly mean wind speed on interannual variability of sea-air CO_2 exchange has been studied before (Olsen et al., 2005). In order to improve the precision of the estimates, wind speed measured on the sampling ship would ideally be used. Since such data were unavailable, reanalysis data, with their associated uncertainty, have been used in this study.

3. Results

3.1. The average annual cycle

The annual cycles features (Fig. 2) are typical of a mid-latitude northern-hemisphere oceanic area. These were obtained by averaging available data over the restricted PAP-SO footprint. Comparing with the annual cycles derived by Frigstad et al. (2015) from the PAP surface mooring, the SST, MLD and nitrate are very similar both in terms of the range and the annual evolution.

The double peak in seawater pCO_2 and CO_2 flux is not however observed in the PAP-derived annual cycles. It is also not observed in the North Atlantic climatology derived by Takahashi et al. (2009). However, this feature was observed in a study in the Bay of Biscay (Jiang et al., 2013). Further decomposition by latitude reveals that the summer peak is mostly driven by measurements in the southern half of the study area, which give an annual cycle closer to a typical subtropical one, while the measurements in the northern half give an annual cycle closer to a typical subpolar record, resembling a sinusoid. The PAP-SO site, where the double peak is not observed, is situated in the northern half.

Nitrate concentrations are highest in the months of January, February, March and April. These winter values are higher than 4 μmol L^{-1}, while the summer values are close to the detection limit, suggesting that nitrate is a limiting nutrient for phytoplankton growth following the spring bloom in this region.

The mixed layer deepens in the winter up to a maximum of over 200 m, while in the summer, it is shallower than 20 m in July and August. The strongest average winds (over 10 m s^{-1}) are recorded in the months of December, January and February and summer values drop to below 7 m s^{-1}.

Features such as a double peak in seawater pCO_2 and CO_2 flux are observed. Carbon uptake is weak at the end of the winter season (February-March) and end of the summer season (August-September). Seawater pCO_2 has the highest average values in the months of February and March at over 370 μatm with a secondary peak in August at just over 360 μatm, while CO_2 flux into the ocean has two peaks in November and May. On average, over 5 mmol m^{-2} day^{-1} of CO_2 enter the surface ocean in the months of November and December.

In the following section, in order to avoid issues related to autocorrelation of the variables, monthly anomalies (seasonally detrended monthly averages) were calculated and used to determine long-term trends.

3.2. Long term variability

Atmospheric pCO_2 calculated from the measured xCO_2 at Mace Head Observatory in Ireland had a mean increase of 2.09 ± 0.03 μatm yr^{-1} ($p < 0.01$) from 2002 to 2016 (Fig. 3a), similar to the rate observed during the last decade at the Mauna Loa Observatory (Earth System Research Laboratory, 2018).

Seawater pCO_2 in our study area however does not follow the same trend (Fig. 3b). There is a small, not statistically significant ($p = 0.09$) rise of 0.37 ± 0.22 μatm yr^{-1} but the amplitude of the seasonal cycles becomes larger in the second half of the time series, with monthly-averaged values in 2003 ranging from 343 to 368 μatm, while the range in 2016 is 336 to 392 μatm. This observation differs from those of Bates et al. (2012) and Takahashi et al. (2009), who found an increasing trend of 1.8 μatm yr^{-1} near Bermuda and of 1.66 to 2.13 μatm yr^{-1} in the NADR, respectively. In a similar study area, McKinley et al. (2011) and Schuster et al. (2009) found seawater pCO_2 trends exceeding the atmospheric one between 1993 and 2005 and 1990 and 2006 respectively. However, it is consistent with other studies where no trend in seawater pCO_2 was observed, such as in the Eastern Tropical Atlantic (Lefèvre et al., 2016). Although in a different study area, where different mechanisms are at play, this study shows that regionally, seawater pCO_2 may not reflect the rise in atmospheric levels. In fact, a recent neural network mapping-based study found that in our study area, observations indicate a lower seawater pCO_2 than predicted by the climatology (Fig. 6 in Landschützer et al., 2014).

There is no statistically significant trend in calculated DIC either (Fig. 3h). Monthly-averaged values range between around 2040 and 2140 μmol kg^{-1}, with a slight increase in the variability in the second half of the time series. Since there is a statistically significant decrease in salinity anomalies with time (−0.018 ± 0.005 yr^{-1}, $p < 0.01$, Fig. 3d), salinity-normalized DIC anomalies (nDIC) show a positive trend (0.68 ± 0.18 μmol kg^{-1} yr^{-1}, $p < 0.01$). This trend is lower than all seven of the carbon time series evaluated by Bates et al. (2014), spanning over various ocean provinces, which show positive trends in nDIC, but with faster increases with time. Their analysis period is also much longer than the present study. The recent freshening of the North Atlantic has been attributed to the interaction of increased freshwater fluxes and subpolar gyre circulation (Tesdal et al., 2018) and can also be a result of the global water cycle intensification (Durack et al., 2012).

Since atmospheric pCO_2 has been increasing and seawater pCO_2 has not, the flux of CO_2 into the ocean has increased by 1.19 ± 0.03 mmol m^{-2} day^{-1} per year ($p < 0.01$, Fig. 3k). Data show the study area acted as a CO_2 source only on a few occasions during the 15 year-long time series (September 2005, September 2006, August 2007, February 2010 and August 2010). Apart from one, all of these instances occurred in late summer, early autumn, at the end of the productive season when atmospheric pCO_2 is at the annual minimum. Data from the nearby PAP observatory show this area is an overall carbon sink (Körtzinger et al., 2008). Consistently, we found an average ± standard deviation CO_2 flux of 1.33 ± 0.71 mol m^{-2} year^{-1} into the ocean, weaker than the flux calculated by Körtzinger et al. (2008) at the PAP-SO site. The PAP-SO sensor had however recorded much lower values of seawater pCO_2 than the SOO. The resulting disequilibrium between the ocean and the atmosphere pCO_2 leads to a strong flux into the ocean. This mismatch between the datasets in 2004 is discussed further in the following section.

Integrated over the 7.9×10^5 km^2 area of the restricted PAP footprint, the 2002–2016 SOO-derived flux yields an uptake of 0.013 Pg C yr^{-1}. This uptake is stronger than the area-weighted estimation of

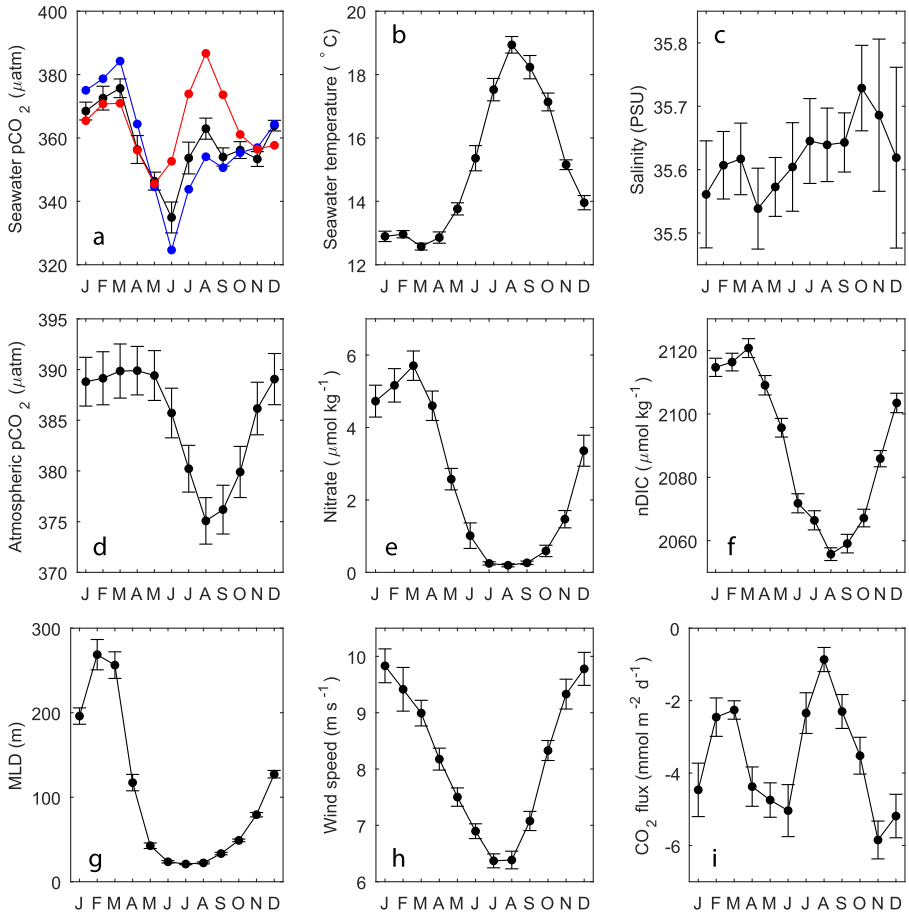

Fig. 2. The annual cycle of several variables used in this study (2002–2016). The error bars show the standard error of the mean for the respective months throughout the period of observations. The seawater pCO_2 cycle (a) is further divided according to sampling location: blue for north of 45° N and red for south of 45° N. Negative CO_2 fluxes (i) indicate a flux from the air to the sea.

Takahashi et al. (2009) for the mid-latitude North Atlantic in the year 2000, but weaker than than the 1985–2010 area-weighted uptake estimated for the 'North Atlantic Subtropical Seasonally Stratified' biome by Rödenbeck et al. (2015).

Since the salinity time series shows no values below 35.4 measured on the UK-Caribbean route before 2011, but multiple in the second part of the time series, including 11 consecutive months below this value, trends were calculated for the 2002–2010 and 2011–2016 periods and synthesised in Table 2. The rise in atmospheric pCO_2 has accelerated with time. On the other hand, the seawater pCO_2 trend was only statistically significant before 2010. As a consequence, the CO_2 flux into the ocean trend only became significant after 2011.

While there is no statistically significant trend in seawater pCO_2 when all the monthly averages are analysed, only using the annual maximum value results in a positive trend of 1.63 ± 0.44 μatm yr^{-1}. This is closer to the atmospheric pCO_2 trend. Several studies use winter observations to detect pCO_2 trends in order to avoid summertime biological activity biases (Fröb et al., 2019; Metzl et al., 2010). At the same time, the average Revelle factor is increasing and thus the buffer factor of the system is decreasing. The long term increase in the Revelle factor is 0.019 ± 0.011, consistent with the time series investigated by Bates et al. (2014), albeit not statistically significant ($p = 0.08$). This means that the amount of pCO_2 change expected to occur for a given change in DIC will be larger (Egleston et al., 2010). Towards the end of the time series, there is a larger difference between the annual seawater pCO_2 maximum (at the end of the winter) and minimum (after the spring bloom). Nitrate concentrations are not higher at this time, but the spring bloom, which to a first order would be expected to draw down DIC in proportion to the amount of nitrate removed, is having an increased influence on the resulting summer pCO_2 decrease. This is consistent with the increased seasonality observed in the pCO_2 time series and visually represented in Fig. 4. The ratio of ΔpCO_2 (μatm) – here used to signify the seasonal winter to summer difference – to ΔNitrate (μmol kg^{-1}) increased with time by 0.31 per year ($p < 0.05$, $R^2 = 0.35$) when one outlier was removed. Recently, Landschützer et al. (2018) found observations that confirmed the predictions of increased atmospheric CO_2 impacting the seasonal cycle of ocean carbon. Consistent with this study, they found an increasing difference between the winter and summer seawater pCO_2.

3.3. Comparison with PAP-SO

A comparison of the footprint-wide data with the ones from the PAP-SO buoy sensors at 1 and 30 m is shown in Fig. 5. Although one of the sensors is located at 30 m, this depth is within the mixed layer for approximately 8 months on any given year. The MLD is shallower than 30 m only between June and September on average. These months are indicated on the comparison plots.

There is good agreement regarding seasonal variability and range for the 2010–2012 and a partially good agreement for the 2013–2016 periods. In 2013 and 2015, the PAP-SO 1 m sensor does not capture the secondary late summer peak in pCO_2 observed by the SOO, while sensor values between September 2014 and February 2015 are questionable since during a storm in mid-September there was a sudden change in values. The PAP sensor values for the 2003–2004 interval show a minimum far below the average SOO values with a difference of over

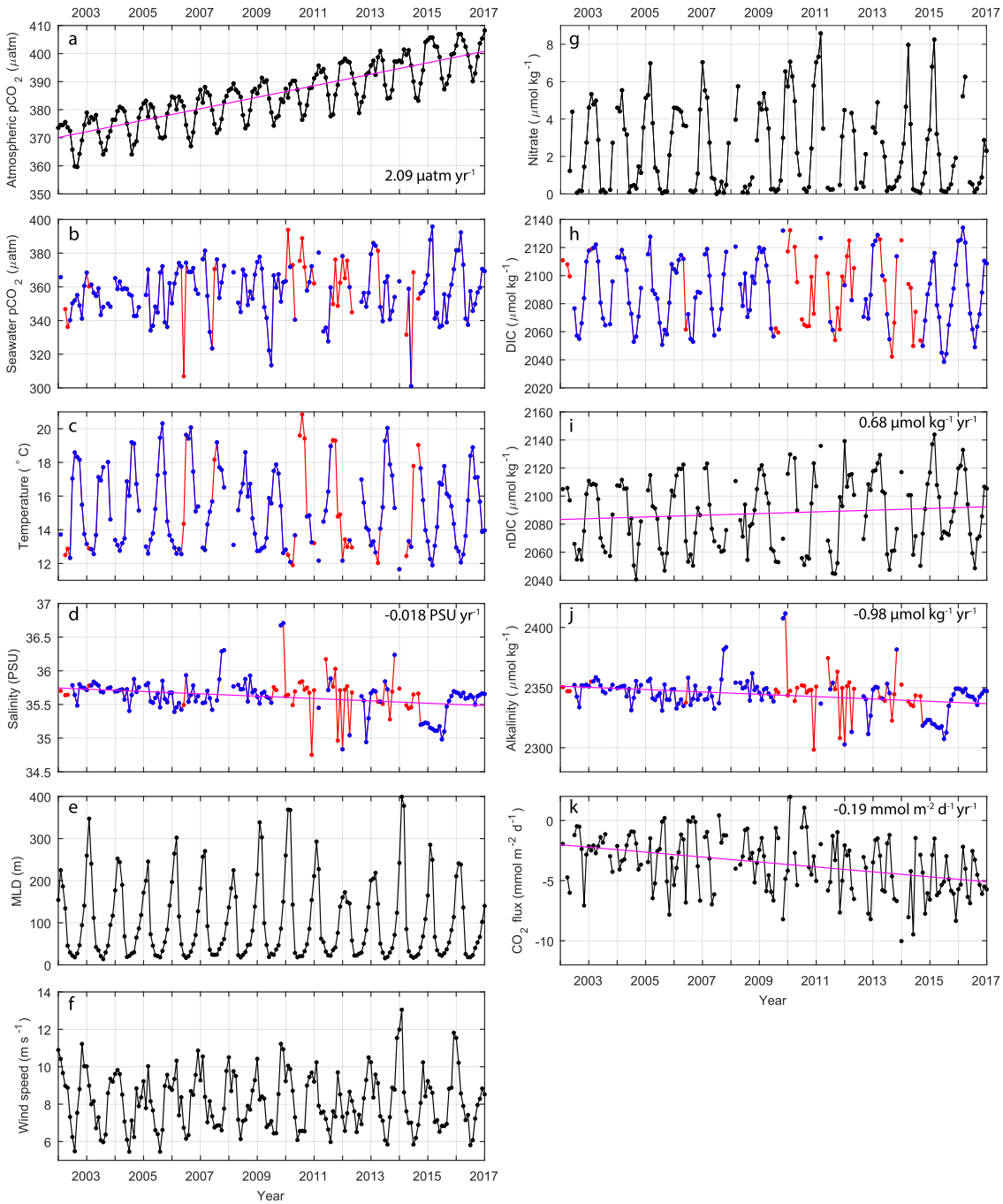

Fig. 3. Monthly averages of atmospheric pCO_2 (a), seawater pCO_2 (b), SST (c), SSS (d), MLD (e), wind speed (f), surface nitrate (g), DIC (h), nDIC (i), alkalinity (j) and CO_2 flux (k). The seawater pCO_2, SST, SSS, DIC and alkalinity blue symbols represent data from the SOO usual route and the red symbols show months when data was filled in from other ships transiting our study area. Statistically significant trends in the monthly anomalies are shown in magenta lines.

Table 2
Trends for selected variables showing the average ± 1 standard deviation (expressed in the units shown in the first column) and annual change where $p < 0.05$ (expressed in the same units per year) for two subsets of the study period, as well as the entire time series.

Variable	2002–2010		2011–2016		2002–2016	
Atmospheric pCO_2 (μatm)	**378.6 ± 7.3**	1.89 ± 0.07	**394.5 ± 7.3**	2.26 ± 0.15	**385.0 ± 10.7**	2.09 ± 0.03
Seawater pCO_2 (μatm)	**357.4 ± 13.5**	1.36 ± 0.48	**357.9 ± 18.6**		**357.6 ± 15.5**	
SSS (PSU)	**35.7 ± 0.2**		**35.5 ± 0.3**		**35.6 ± 0.3**	−0.018 ± 0.005
nDIC (μmol kg^{-1})	**2086.4 ± 23.0**		**2091.6 ± 27.1**		**2088.5 ± 24.9**	0.68 ± 0.18
Alkalinity (μmol kg^{-1})	**2348.2 ± 13.7**		**2338.5 ± 16.2**		**2344.3 ± 15.9**	−0.98 ± 0.27
Revelle factor	**10.66 ± 0.50**		**10.84 ± 0.64**		**10.72 ± 0.56**	
CO_2 flux (mmol m^{-2} day^{-1})	**− 2.9 ± 2.1**		**− 4.8 ± 2.0**	−0.25 ± 0.12	**− 3.6 ± 2.2**	−0.19 ± 0.03

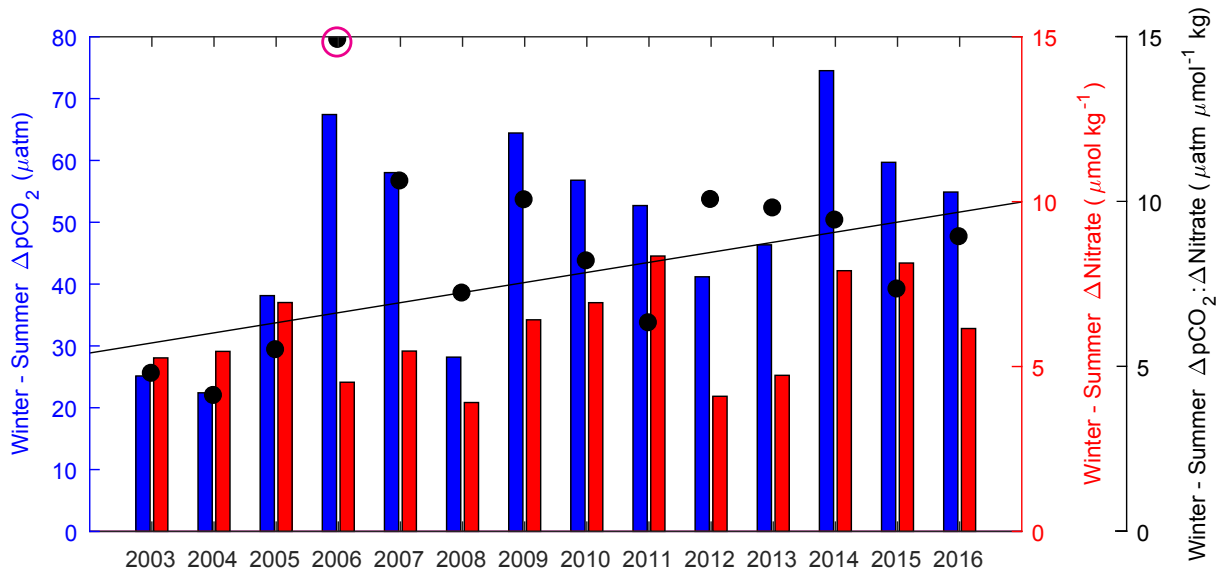

Fig. 4. The annual difference between winter maximum and summer minimum seawater pCO_2 (nitrate) represented by the blue (red) bars and shown on the left (right) vertical axis. The ratio of ΔpCO_2 to ΔNitrate is represented by the black symbols and shown on the secondary right vertical axis. One outlier was removed from the long term trend analysis.

40 µatm, but many of the measurements were taken when the sensor was outside the shallow summer mixed layer. The PAP sensor data for the 2003–2004 interval is deemed correct for the PAP location as it has been calibrated against pCO_2 derived from direct DIC and total alkalinity measurements (Körtzinger et al., 2008). Perhaps the seasonal variability has increased in the second part of the time series because the SOO sensor was not capturing the same signal as the 30 m PAP sensor in the early years. The lowest number of SOCAT observations in our study area are recorded in this 2003–2004 interval, which might be an additional reason for the mismatch. Even with a mismatch in the pCO_2 comparison, the nDIC from the ship and the PAP site show a strong correspondence. DIC is calculated from pCO_2 and alkalinity. Similar results with different pCO_2 inputs highlight the greater weighting factor of alkalinity compared to pCO_2 in this calculation. Although being derived through different methods, the SOO and PAP site nDIC are very similar.

We investigated the influence of the differences between the two data sets on our CO_2 flux calculations. Monthly averages were computed for the PAP 1 m sensor data in order to directly compare and compute fluxes (as described earlier). For the 18 months when data was available from both sources (excluding the 2014 period affected by the storm), the average CO_2 flux into the ocean was 4.54 and 5.90 mmol m^{-2} day^{-1} when calculated with the SOO and the PAP data respectively. The relevance of this difference depends on the questions being addressed and the required accuracy. For our study, we find the agreement satisfactory in order to strengthen our conclusion that the area around the PAP site has remained a strong carbon sink region.

4. Discussion

Despite displaying a larger seasonal variability in the second part of the time series, seawater pCO_2 does not follow the rising trend of atmospheric pCO_2 and instead does not show a statistically significant trend. This finding has implications for the ability of this area of the ocean to remain a carbon sink, as it has been previously identified, in the context of increasing atmospheric forcing. In order to determine the reason behind this behaviour, we looked at the individual factors exerting control on seawater pCO_2. Seawater pCO_2 is mainly a function of temperature, salinity, DIC concentration and alkalinity (Takahashi et al., 1993). Tjiputra et al. (2014) found that DIC is the dominant

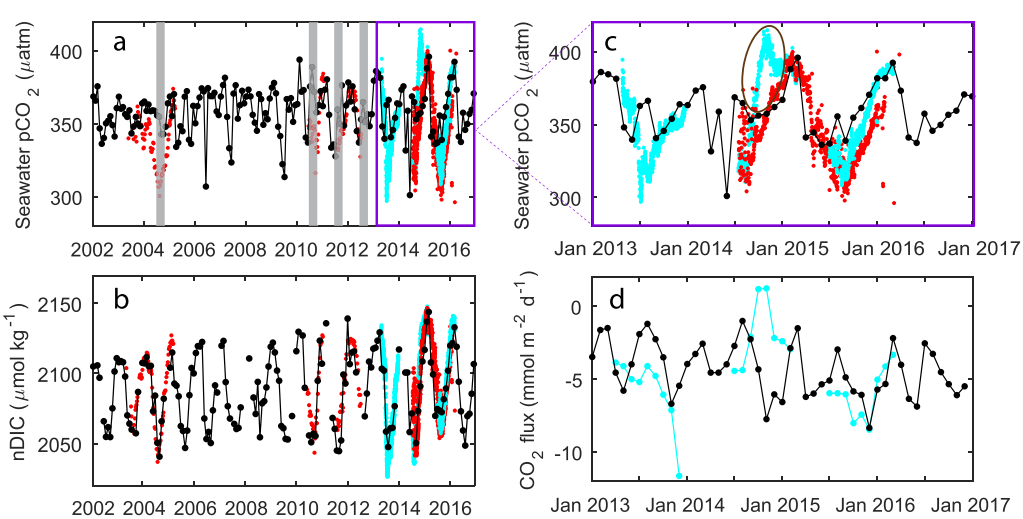

Fig. 5. (a) Comparison between the spatially and temporally-averaged pCO_2 from the SOO (black symbols) and the pCO_2 recorded by the 1 m (cyan symbols) and 30 m depth (red symbols) sensors on the PAP buoy. Grey bars cover months when the 30 m sensor is outside the mixed layer (b) Same as above, but for salinity-normalised DIC. (c) Zoom-in on the 2013–2016 period in sub-figure a. The period where the 1 m sensor was affected by a storm is shown in the brown oval. (d) Comparison between the CO_2 flux calculated using the SOO pCO_2 and the flux calculated with monthly-averaged PAP 1 m sensor pCO_2.

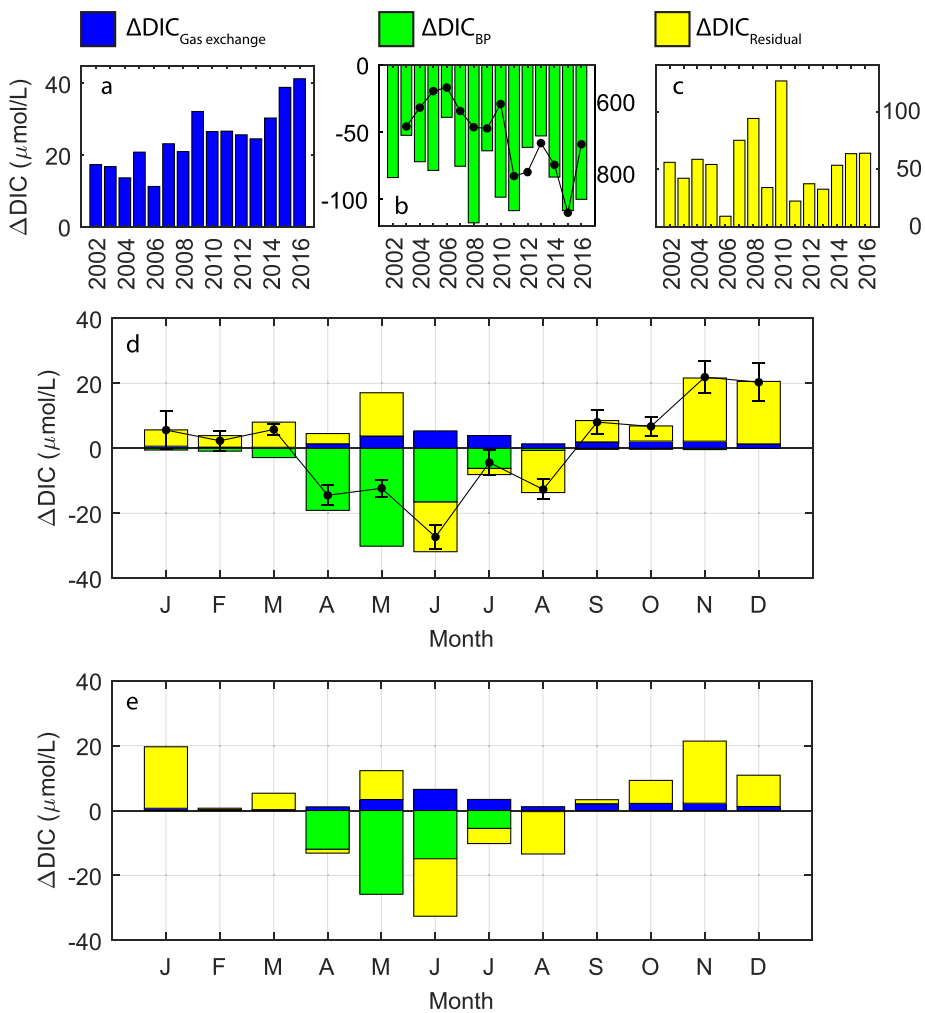

Fig. 6. Annual sum of the monthly contributions of gas exchange (a), biological production (b) and the residuals (c) to the nDIC changes (all bars in μmol L^{-1}); the long-term average nDIC monthly contributions with the average monthly nDIC change plotted in black symbols on top (d); the nDIC monthly contributions predicted from the typical annual cycle in Fig. 2 (e). Subfigure (b) also shows the annual average NPP (mg m^{-2} day^{-1}) on a reversed y-axis.

driver of pCO_2 changes. We therefore first investigate what causes changes in surface nDIC.

4.1. Processes affecting nDIC

DIC concentration is determined by physical and biological processes. Gas exchange affects it through the dissolution of carbon dioxide in seawater (Park, 1969). Influx of CO_2 into the sea increases the DIC concentration. DIC is consumed by phytoplankton during the productive season and replenished during winter through mixing/convection (Shadwick et al., 2011). Following calculations explained in Section 2.2, in Fig. 6a and b, we present monthly contributions of variables to nDIC.

Our assessment reveals DIC changes due to gas exchange increased with time (Fig. 6a), corresponding to the increasing ΔpCO_2. There is a statistically significant ($p < 0.01$) trend of 1.8 ± 0.3 μmol L^{-1} per year in the yearly contribution between 2003 and 2016, the complete data years. This is more than 7% of the average yearly sum of 25.2 μmol L^{-1} – the contribution of gas exchange to the nDIC concentrations. $\Delta DIC_{Gas\ exchange}$ is largest in May, June and July (Fig. 6d). These are the months that on average have the lowest seawater pCO_2 values (Fig. 2a) resulting in large ΔpCO_2. In addition, the same months also have shallow MLD (Fig. 2g) so, according to Eq. (4), the gas exchange contribution will be greater.

The ΔDIC_{BP} terms show a trend of − 2.4 ± 1.5 μmol L^{-1} per year, albeit not statistically significant – more than 3% of the − 79.6 μmol L^{-1} average yearly sum of the ΔDIC_{BP} contributions. The monthly nitrate concentrations and average MLD do not show a statistically significant trend during our study period, so the ΔDIC_{BP} changes are likely caused by a change in the timing of the spring bloom. Palevsky and Quay (2017) found that the seasonal timing of net community production strongly influences the effect on air-sea CO_2 flux. Earlier onsets of the decrease in nitrate, during the months when MLD is deeper, lead to greater integrated ΔDIC_{BP} values according to Eq. (5). The contribution of the ΔDIC_{BP} is largest in 2008, 2011 and 2015. While nitrate concentrations were high in the winter season before the productive season in 2011 and 2014, the large value in 2008 is driven by the relatively shallow MLD of that year. For 2011 and 2015 this is coherent with independent net primary productivity (NPP) derived from satellite.

The strongest uptake of DIC is observed during the spring bloom in the months of April, May and June with average DIC changes of around 20 μmol L^{-1} per month. It is not uncommon for biological production to have an influence on the carbonate system. In the Eastern North Pacific, DIC removal by net community production more than fully offsets the DIC increase due to air-sea gas exchange (Palevsky and Quay, 2017). The increase in the importance of the biological term is consistent with the increase in NPP observed in this region (black symbols in Fig. 6b – note the reversed axis).

The $\Delta DIC_{Residual}$ term annual contribution (Fig. 6c) is positive every

year since it includes the influence of wintertime vertical mixing, which brings up DIC from the deep waters. The reventilated CO_2 produced by subsurface respiration was found to negate more than one third of the carbon drawdown by net community production at the PAP site (Körtzinger et al., 2008). Other contributions to the $\Delta DIC_{Residual}$ are likely due to horizontal advection as well as the propagation of the combined uncertainty of the terms used in the calculations.

Fig. 6d and e show the average annual cycle of the contributions from the individual monthly contributions and from the mean annual cycle presented in Fig. 2. While mostly similar, some differences are seen in the magnitude of the wintertime $\Delta DIC_{Residual}$ terms and the absence of wintertime ΔDIC_{BP} term when the mean annual cycle is used. The rare occurrences of nitrate decreasing between two consecutive autumn/winter months and causing a ΔDIC_{BP} contribution are eliminated when using the typical annual cycle.

In our study, during an average year, the $\Delta DIC_{Residual}$ term accounts for 68.9% of the total changes in the nDIC concentration. This is a large value, but much of the contribution is given by winter mixing of DIC-rich water.

4.2. Processes affecting pCO_2

As discussed above, the calculated changes in nDIC were used to determine their respective influence on pCO_2. The terms that cause an increase (a decrease) in surface nDIC concentration also cause a proportional increase (decrease) in pCO_2. Decomposing the nDIC contributions in the previous section allows us to decompose the pCO_2 contributions in more detail than just using temperature, alkalinity and DIC changes.

In addition to the terms discussed above, the temperature influence is introduced as a new term ($\Delta pCO_2\,(Temp)$). The individual monthly contributions as well as the typical annual cycle are shown in Fig. 7. The warm summer temperatures cause a rise in pCO_2 between the months of April and August and the reverse is true for the colder temperatures between September and March. The sum of the average temperature contribution during the April-August period would cause an increase of surface pCO_2 of 112 µatm. This is however balanced by the 106 µatm opposing change forced by biological production during the same period. Fay and McKinley (2017) found the $\Delta pCO_2\,(Temp)$ term is more important for the pCO_2 seasonality in the subtropics, while the $\Delta pCO_2\,(\Delta DIC_{BP})$ becomes more important in the subpolar areas. The PAP footprint lies in the mid-latitude ocean, between the subtropical and subpolar areas and it appears that these two terms are of similar magnitude, which is consistent with the conclusions of Takahashi et al. (2002). For our entire study period and study area there is no significant change in annual average SST. Between 2005 and 2014 however, there is a small decrease of $-\ 0.07\ \pm\ 0.03\ ^{\circ}C\ yr^{-1}$, consistent with the findings of Robson et al. (2016), who identified a cooling and freshening of the upper ocean over the 2005–2014 period in the northeast Atlantic, where our study area is situated. It has been shown however that the effect of large temperature differences between winter and summer is more important than the maximum temperature reached during the summer. Strong warming in the transition from the winter to the summer seasons can indeed outweigh the effect of intense phytoplankton blooms (Dumousseaud et al., 2010).

The influence of changes in alkalinity only produces a strong signal in years when there are rapid changes in alkalinity between two consecutive months. Because our derived alkalinity is largely related to SSS, these coincide with changes in salinity.

There is a statistically significant increasing trend in the annual sum of the $\Delta pCO_2\,(\Delta DIC_{Gas\ Exchange})$ term of $3.1\ \pm\ 0.5$ µatm yr^{-1}. This is due to the increasing difference between the atmospheric and seawater pCO_2 and not due to increasing wind speed, which shows no significant trend in our analysis. Although future projections estimate an increase in global wind speed, only the magnitude, not the direction of the flux will be affected (Wanninkhof and Triñanes, 2017). Both sink and source areas are estimated to become stronger.

The difference between the observed changes in pCO_2 and the sum of the contributions of temperature, alkalinity and various DIC changes has been assigned to the $\Delta pCO_2\,(Residual)$ term. In years such as 2010, when some data are missing from the main UK-Caribbean route, this term is larger since the sum of the calculated terms does not match some of the abrupt changes observed between consecutive months in the SOCAT database. Although for an average year, this residual term only accounts for 23.4% of the total contribution, it is negative in all but one of the years of the time series (i.e. 2009), which implies there exists a sum of unknown processes lowering pCO_2. It appears that part of the reason the seawater pCO_2 does not show an increment during our study period is due to this additional term.

4.3. Carbon to nitrogen stoichiometry and nitrate-pCO_2 relationship

To further investigate the effect of new production on the carbonate system variables, we focus on the spring bloom months. The PAP footprint area exhibits annual cycling typical of a mid-latitude Northern Hemisphere oceanic region (Wong et al., 2002). We work under the assumptions that the April, May and June months represent the bloom period since nitrate concentrations decrease abruptly. The nitrate concentrations are on average below 0.7 µmol L^{-1} during July, August, September and October. The average SST is above 16 °C during these months, which were grouped together as the 'post-bloom' period. The remaining months were defined as the 'pre-bloom' period. We thus used the same notation as Jiang et al. (2013) in grouping the months around the timing of the bloom.

In this study we used a C:N ratio of 6.6 (i.e. Redfield ratio) to determine the influence of biological production on nDIC concentrations. There are studies however that suggest carbon overconsumption occurs in the North Atlantic (Koeve, 2004; Sambrotto et al., 1993; Toggweiler, 1993). The gas-corrected nDIC ($\Delta DIC_{Gas\ exchange}$ excluded) and nitrate concentrations in our study are linearly correlated ($R^2 = 0.37$, $p < 0.01$) during the 'bloom' months (blue symbols in Fig. 8a). The slope of this line, obtained by ignoring nitrate values < 0.5 µmol L^{-1} similarly to the method used by Jiang et al. (2013), is $6.2\ \pm\ 1.6$, similar to the canonical Redfield ratio. While we found no evidence for carbon overconsumption when using the data within the restricted PAP footprint, performing the same calculations with data from the whole NADR (a rectangular box between 42 and 55° N and 10 and 42° W) revealed a C:N ratio of $9.6\ \pm\ 1.4$, a value similar to that found in a study in the Iceland Sea (Jeansson et al., 2015). In both cases it seems likely remineralisation occurs within the mixed layer since the 'pre-bloom' (red symbols in Fig. 8a) have a similar trendline, indicating a comparable C:N ratio during the wintertime mixing.

In Fig. 2a we showed that the annual seawater pCO_2 displays a double peak distribution with high values in winter as well as late summer. This behaviour has also been reported by Jiang et al. (2013) in the Bay of Biscay. While subtropical regions display a distribution with a single summer maximum due to the temperature control (Bates et al., 1996), the DIC variations are the main driving factor for pCO_2 leading to a single winter peak in subpolar regions (Olsen et al., 2008). The double peak in our study area suggests that both controls are important, consistent with past studies (Takahashi et al., 2002). Winter mixing of DIC and nitrate-rich water coincides with the increase in pCO_2, which is then removed by spring biological production. Warming in the summer season then increases pCO_2 without a corresponding increase in nitrate. The temperature-driven range of pCO_2 values during the 'post-bloom' summer period in Fig. 8b is similar but slightly smaller compared to the biological production and remineralization-driven range of the 'pre-bloom' and 'bloom' values. While the maximum pCO_2 value reached due to summer warming is smaller than 380 µatm, the winter upwelling of DIC-rich water makes the surface seawater pCO_2 reach almost 400 µatm. These results are consistent with a recent study that found the subpolar North Atlantic ΔpCO_2 to be predominantly correlated with

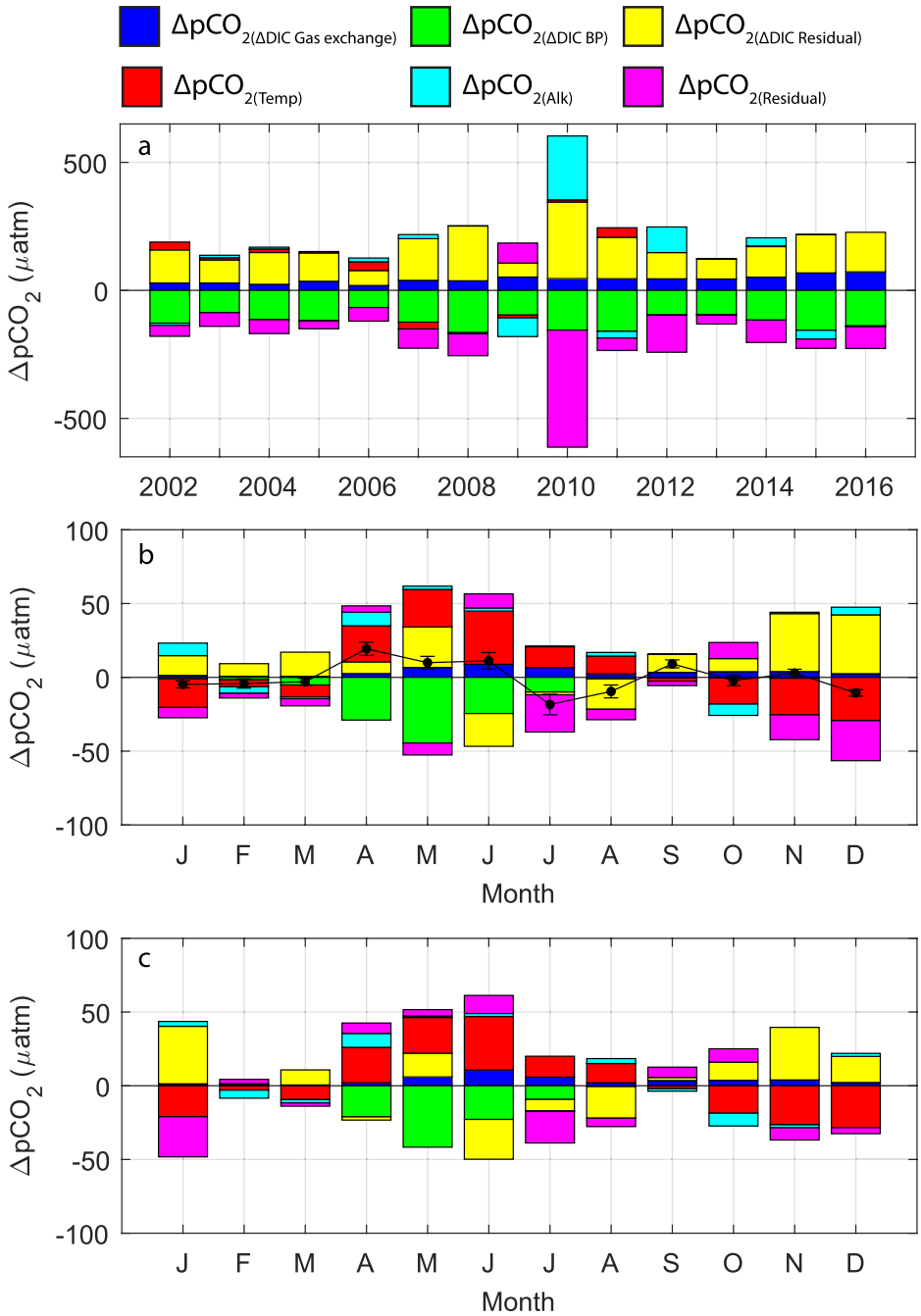

Fig. 7. The annual sum of the monthly contributions to seawater pCO_2 (a); the long-term average pCO_2 monthly contributions with the average monthly pCO_2 change plotted in black symbols on top (b); the pCO_2 monthly contributions predicted from the typical annual cycle in Fig. 2 (c).

biological processes and the subtropical gyre ΔpCO_2 with temperature on seasonal time scales (Henson et al., 2018).

4.4. The residual terms

Around 23% of the annual average seawater pCO_2 observed changes are not explained by the individual terms calculated in this study. Part of the difference could be due to using atmospheric reanalysis products and estimated (rather than measured) alkalinity. To allow inter-comparison, all the terms are converted into monthly averages which might introduce further error if the study area is not homogeneous over its surface. This study does not calculate the influence of advection, which is known to change carbon concentrations in the water column (Fröb et al., 2018). Lateral advection in the subpolar gyre can increase DIC concentrations on a similar magnitude to air-sea gas exchange (Zunino et al., 2015). However, advection can also increase carbon storage if the water that recently absorbed atmospheric CO_2 is moved to a mode water formation site (Andersson et al., 2013). The influence of calcification is also not included in this study. Calcification consumes DIC, but is a CO_2 source (Frankignoulle and Canon, 1994; Shutler et al., 2013). However, with no direct measurements, the influence of calcification would need to be determined through proxies such as using the particulate inorganic carbon to particulate organic carbon ratio (PIC:POC). This estimation has a high uncertainty and a small relative influence on the seawater pCO_2 (Palevsky and Quay, 2017). A recent study found that the presence in the surface water of biological surfactants can reduce gas exchange by up to 32% due to the influence on the gas transfer velocity (Pereira et al., 2018). In our calculations of CO_2 flux, the

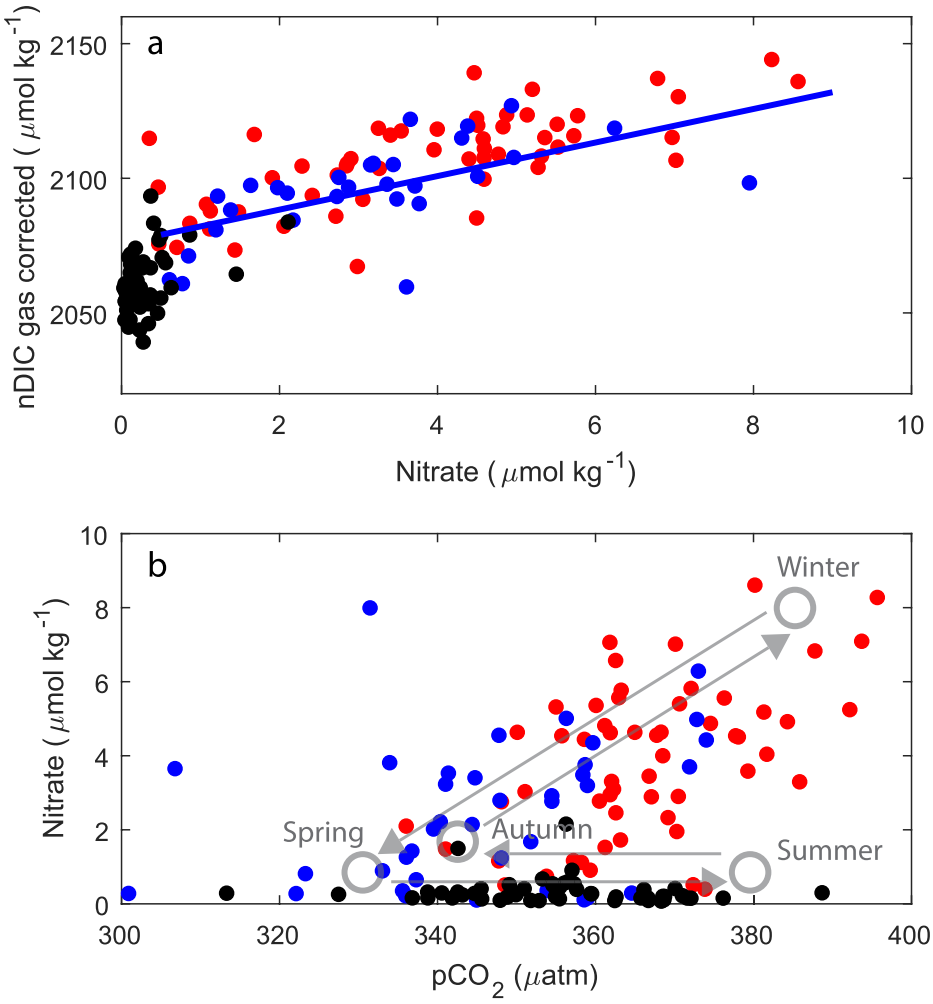

Fig. 8. Scatter plots of gas-corrected nDIC versus nitrate (a) and nitrate versus pCO_2 (b). The red, blue and black symbols correspond to values measured or calculated for the 'pre-bloom', 'bloom' and 'post-bloom' months respectively. The blue line is the C:N regression for the 'bloom' period. Subfigure (b) contains a conceptual visualisation of the inter-seasonal changes.

surfactant influence on k is not accounted for in Eq. (3). While a decrease of the gas flux into the ocean would move the system in the right direction in order to explain some of the $\Delta pCO_2(Residual)$ term, the $\Delta pCO_2(\Delta DIC_{Gas\ Exchange})$ contributes on average only 4.7% to the observed changes so a small change to it would not be enough. Whichever way we decompose the reasons for the variability, the key finding that our observations show us is the relatively stable annual mean seawater pCO_2. A more sophisticated decomposition model, which would include terms not addressed in the current work, would be dedicated to another study.

5. Conclusion

In this study we used SOO observational data to show that the mid latitude North Atlantic Ocean around the PAP site remained a sink for atmospheric CO_2 in recent years. There is good agreement between SOO and fixed-point observatory data for the 15 year time series presented here. The study expands on previous work and constrains the relative contribution of physical and biological factors to observed changes in seawater DIC and pCO_2. The annual average surface seawater pCO_2 showed no statistically significant increasing trend in the area around the PAP-SO site between 2002 and 2016 in spite of the observed increase in atmospheric pCO_2 and nDIC. This meant that the carbon sink capacity was maintained, especially due to the summer time pCO_2 deficit driven by biological processes. Consistent with other recent studies, the difference between winter and summer seawater pCO_2 values became larger during the study period, without a similar change for nitrate. Gas exchange, biological production, temperature and alkalinity changes explained over 76% of the annual pCO_2 variability in the study area.

We are now observing the ocean at a higher resolution than ever before. Using floats and unmanned autonomous vehicles has the potential to add the depth dimension to our observational capacity and also to reach areas where meteorological conditions hinder vessel-based observations. In addition, observations have now extended over climatologically significant time scales. In some cases however, even two decades of observations were deemed insufficient to investigate a relationship with decadal variability (Midorikawa et al., 2006). In much of the ocean, long term signals require a much longer period of observations than what is available in this study (McKinley et al., 2016). Continuous monitoring will improve our understanding of the carbonate system and help guide our future predictions.

By the end of the 21st century, the ocean carbon sink is expected to weaken overall since the effect of nutrient limitation will outweigh the effect of a longer growing season (Henson et al., 2013). The amount of CO_2 uptaken will determine the driving mechanisms for the North Atlantic carbon system. It has been modelled that in a low anthropogenic carbon uptake world, SST will be dominating the annual cycle of seawater pCO_2, while mixing and biological production will be dominant in a high anthropogenic uptake world (Goris et al., 2018). It

is clear that without a solid understanding of the constrains to the marine carbon cycle, our ability to confidently predict the status of the global ocean carbon sink under increased atmospheric forcing will be limited.

Declaration of Competing Interest

The authors declare no conflict of interest. Sources of funding have been acknowledged.

Acknowledgements

We thank the two anonymous reviewers whose comments/suggestions helped improve and clarify this manuscript. We would like to thank the following individuals and organizations: the captains, officers, and crews of MV *Santa Lucia*, MV *Santa Maria* and MV *Benguela Stream* for continuous technical assistance and support on board the ships; staff of Geest Line, U.K., and Seatrade Reefer Chartering, Belgium, for supporting the project; Jon Campbell for collating and processing PAP sensor pCO_2 data. Recent work on the line has been supported by the NERC Greenhouse Gas TAP NE/k00249x/1 project and the Climate Linked Atlantic Sector Science (CLASS) NE/R015953/1 project. The Surface Ocean CO_2 Atlas (SOCAT) is an international effort, endorsed by the International Ocean Carbon Coordination Project (IOCCP), the Surface Ocean Lower Atmosphere Study (SOLAS) and the Integrated Marine Biosphere Research (IMBeR) program, to deliver a uniformly quality-controlled surface ocean CO_2 database. The many researchers and funding agencies responsible for the collection of data and quality control are thanked for their contributions to SOCAT (https://www.socat.info). Both the SOO and the PAP observatory are ICOS sites (https://www.icos-ri.eu/). PAP is also an EMSO site (https://emso.eu/). Sue Hartman received funding from Horizon 2020, EU Project "EMSO-Link" grant ID 731036. This work was supported by the Natural Environmental Research Council [Grant No. NE/L002531/1].

References

Alduchov, O.A., Eskridge, R.E., 1996. Improved magnus form approximation of saturation vapor pressure. J. Appl. Meteorol. 35, 601–609. https://doi.org/10.1175/1520-0450(1996) 035<0601:imfaos>2.0.co;2.

Andersson, A.J., Krug, L.A., Bates, N.R., Doney, S.C., 2013. Sea-air CO2 flux in the North Atlantic subtropical gyre: role and influence of Sub-Tropical Mode Water formation. Deep-Sea Res. Part II-Top. Stud. Oceanogr. 91, 57–70. https://doi.org/10.1016/j.dsr2.2013.02.022.

Bakker, D.C.E., Lauvset, S.K., Wanninkhof, R., Castaño-Primo, R., Currie, K.I., Jones, S.D., Landa, C.S., Metzl, N., Nakaoka, S.I., Nojiri, Y., Nonaka, I., O'Brien, K.M., Olsen, A., Pfeil, B., Pierrot, D., Schuster, U., Smith, K., Sullivan, K., Sutton, A., Tilbrook, B., Alin, S.R., Becker, M., Benoit-Cattin, A., Bott, R., Bozec, Y., Bozzano, R., Burger, E.F., Burgers, T., Cai, W.J., Chen, L., Chierici, M., Corredor, J.E., Cosca, C.E., Cross, J., Dandonneau, Y., De Carlo, E.H., Dietrich, C., Else, B., Emerson, S.R., Farias, L., Fransson, A., Garreaud, R.D., Gkritzalis, T., Glockzin, M., González-Dávila, M., Gregor, L., Hartman, S.E., Hermes, R., Hoppema, M., Howden, S., Hunt, C.W., Hydes, D., Ibánhez, J.S.P., Kitidis, V., Körtzinger, A., Kozyr, A., Kuwata, A., Lampitt, R.S., Lefèvre, N., Lo Monaco, C., Maenner, S.M., Manke, A., Manzello, D.P., McGillis, W., Mickett, J., Monteiro, P.M.S., Morell, J.M., Morrison, R., Mucci, A., Munro, D.R., Musielewicz, S., Negri, R.M., Newberger, T., Newton, J., Noakes, S., O'Brien, C., Ólafsdóttir, S.R., Ólafsson, J., Ono, T., Osborne, J., Ouyang, Z., Padín, X.A., Papakyriakou, T.N., Plüddemann, A.J., Rehder, G., Sabine, C.L., Sakurai, K., Salisbury, J., Santana-Casiano, J.M., Schlitzer, R., Schneider, B., Send, U., Skjelvan, I., Steinhoff, T., Sulpis, O., Sutherland, S.C., Sweeney, C., Tadokoro, K., Takahashi, T., Telszewski, M., et al., 2018. Surface Ocean CO2 Atlas (SOCAT) V6. doi: https://doi.org/10.1594/PANGAEA.890974, doi: https://doi.org/10.1594/PANGAEA.890974.

Bates, N.R., Astor, Y.M., Church, M.J., Currie, K., Dore, J.E., Gonzalez-Davila, M., Lorenzoni, L., Muller-Karger, F., Olafsson, J., Santana-Casiano, J.M., 2014. A time-series view of changing surface ocean chemistry due to ocean uptake of anthropogenic CO2 and ocean acidification. Oceanography 27, 126–141. https://doi.org/10.5670/oceanog.2014.16.

Bates, N.R., Best, M.H.P., Neely, K., Garley, R., Dickson, A.G., Johnson, R.J., 2012. Detecting anthropogenic carbon dioxide uptake and ocean acidification in the North Atlantic Ocean. Biogeosciences 9, 2509–2522. https://doi.org/10.5194/bg-9-2509-2012.

Bates, N.R., Michaels, A.F., Knap, A.H., 1996. Seasonal and interannual variability of oceanic carbon dioxide species at the U.S. JGOFS Bermuda Atlantic Time-series Study (BATS) site. Deep Sea Res. Part II: Top. Stud. Oceanogr. 43, 347–383. https://doi.org/10.1016/0967-0645(95)00093-3.

Behrenfeld, M.J., Falkowski, P.G., 1997. Photosynthetic rates derived from satellite-based chlorophyll concentration. Limnol. Oceanogr. 42, 1–20.

Broecker, W.S., Takahashi, T., Simpson, H.J., Peng, T.H., 1979. Fate of fossil fuel carbon dioxide and the global carbon budget. Science 206, 409. https://doi.org/10.1126/science.206.4417.409.

Clargo, N.M., Salt, L.A., Thomas, H., de Saar, H.J.W., 2015. Rapid increase of observed DIC and pCO(2) in the surface waters of the North Sea in the 2001–2011 decade ascribed to climate change superimposed by biological processes. Mar. Chem. 177, 566–581. https://doi.org/10.1016/j.marchem.2015.08.010.

Dee, D.P., Uppala, S.M., Simmons, A.J., Berrisford, P., Poli, P., Kobayashi, S., Andrae, U., Balmaseda, M.A., Balsamo, G., Bauer, P., Bechtold, P., Beljaars, A.C.M., van de Berg, L., Bidlot, J., Bormann, N., Delsol, C., Dragani, R., Fuentes, M., Geer, A.J., Haimberger, L., Healy, S.B., Hersbach, H., Holm, E.V., Isaksen, L., Kallberg, P., Kohler, M., Matricardi, M., McNally, A.P., Monge-Sanz, B.M., Morcrette, J.J., Park, B.K., Peubey, C., de Rosnay, P., Tavolato, C., Thepaut, J.N., Vitart, F., 2011. The ERA-Interim reanalysis: configuration and performance of the data assimilation system. Quart. J. Roy. Meteorol. Soc. 137, 553–597. https://doi.org/10.1002/qj.828.

Derwent, R.G., Ryall, D.B., Manning, A.J., Simmonds, P., O'Doherty, S., Biraud, S., Ciais, P., Ramonet, M., Jennings, S.G., 2002. Continuous observations of carbon dioxide at Mace Head, Ireland from 1995 to 1999 and its net European ecosystem exchange. volume 36. doi: https://doi.org/10.1016/S1352-2310(02)00203-0.

Dickson, A., Wesolowski, J.D., Palmer, D., Mesmer, E.R., 1990. Dissociation Constant of Bisulfate Ion in Aqueous Sodium Chloride Solutions to 250C, vol. 94. doi: https://doi.org/10.1021/j100383a042.

Doney, S.C., Fabry, V.J., Feely, R.A., Kleypas, J.A., 2009. Ocean acidification: the other CO2 problem. Ann. Rev. Mar. Sci. 1, 169–192. https://doi.org/10.1146/annurev.marine.010908.163834.

Dumousseaud, C., Achterberg, E.P., Tyrrell, T., Charalampopoulou, A., Schuster, U., Hartman, M., Hydes, D.J., 2010. Contrasting effects of temperature and winter mixing on the seasonal and inter-annual variability of the carbonate system in the Northeast Atlantic Ocean. Biogeosciences 7, 1481–1492. https://doi.org/10.5194/bg-7-1481-2010.

Durack, P.J., Wijffels, S.E., Matear, R.J., 2012. Ocean salinities reveal strong global water cycle intensification during 1950 to 2000. Science 336, 455. https://doi.org/10.1126/science.1212222.

Earth System Research Laboratory, 2018. Trends in atmospheric carbon dioxide. URL https://www.esrl.noaa.gov/gmd/ccgg/trends/.

Egleston, E.S., Sabine, C.L., Morel, F.M.M., 2010. Revelle revisited: buffer factors that quantify the response of ocean chemistry to changes in DIC and alkalinity. Global Biogeochem. Cycles 24. https://doi.org/10.1029/2008GB003407.

Fassbender, A.J., Sabine, C.L., Palevsky, H.I., 2017. Nonuniform ocean acidification and attenuation of the ocean carbon sink. Geophys. Res. Lett. 44, 8404–8413. https://doi.org/10.1002/2017GL074389.

Fay, A.R., McKinley, G.A., 2014. Global open-ocean biomes: mean and temporal variability. Earth Syst. Sci. Data 6, 273–284. https://doi.org/10.5194/essd-6-273-2014.

Fay, A.R., McKinley, G.A., 2017. Correlations of surface ocean pCO2 to satellite chlorophyll on monthly to interannual timescales. Global Biogeochem. Cycles 31, 436–455. https://doi.org/10.1002/2016GB005563.

Frankignoulle, M., Canon, C., 1994. Marine calcification as a source of carbon-dioxide - positive feedback of increasing atmospheric CO2. Limnol. Oceanogr. 39, 458–462. https://doi.org/10.4319/lo.1994.39.2.0458.

Fröb, F., Olsen, A., Becker, M., Chafik, L., Johannessen, T., Reverdin, G., Omar, A., 2019. Wintertime fCO2 variability in the Subpolar North Atlantic since 2004. Geophys. Res. Lett. 46, 1580–1590. https://doi.org/10.1029/2018GL080554.

Fröb, F., Olsen, A., Perez, F.F., Garcia-Ibanez, M.I., Jeansson, E., Omar, A., Lauvset, S.K., 2018. Inorganic carbon and water masses in the Irminger Sea since 1991. Biogeosciences 15, 51–72. https://doi.org/10.5194/bg-15-51-2018.

Frigstad, H., Henson, S.A., Hartman, S.E., Omar, A.M., Jeansson, E., Cole, H., Pebody, C., Lampitt, R.S., 2015. Links between surface productivity and deep ocean particle flux at the Porcupine Abyssal Plain sustained observatory. Biogeosciences 12, 5885–5897. https://doi.org/10.5194/bg-12-5885-2015.

Goris, N., Tjiputra, J.F., Olsen, A., Schwinger, J., Lauvset, S.K., Jeansson, E., 2018. Constraining projection-based estimates of the future North Atlantic carbon uptake. J. Clim. 31, 3959–3978. https://doi.org/10.1175/JCLI-D-17-0564.1.

Gruber, N., Keeling, C.D., Bates, N.R., 2002. Interannual variability in the North Atlantic Ocean carbon sink. Science 298, 2374–2378. https://doi.org/10.1126/science.1077077.

Hartman, S.E., Hydes, D.J., Hemmings, J.C.P., Schuster, U., 2010. Spatial and temporal variation in surface nitrate concentrations in the temperate and sub-tropical North Atlantic. Norrköping.

Hartman, S.E., Jiang, Z.P., Turk, D., Lampitt, R.S., Frigstad, H., Ostle, C., Schuster, U., 2015. Biogeochemical variations at the Porcupine Abyssal Plain sustained observatory in the northeast Atlantic Ocean, from weekly to inter-annual timescales. Biogeosciences 12, 845–853. https://doi.org/10.5194/bg-12-845-2015.

Henson, S.A., Beaulieu, C., Lampitt, R.S., 2016. Observing climate change trends in ocean biogeochemistry: when and where. Glob. Change Biol. 22, 1561–1571. https://doi.org/10.1111/gcb.13152.

Henson, S.A., Cole, H., Beaulieu, C., Yool, A., 2013. The impact of global warming on seasonality of ocean primary production. Biogeosciences 10, 4357–4369. https://doi.org/10.5194/bg-10-4357-2013.

Henson, S.A., Humphreys, M.P., Land, P.E., Shutler, J.D., Goddijn-Murphy, L., Warren, M., 2018. Controls on open-ocean North Atlantic Delta pCO2 at seasonal and interannual time scales are different. Geophys. Res. Lett. 45, 9067–9076. https://doi.org/10.1029/2018GL078797.

Henson, S.A., Sanders, R., Allen, J.T., Robinson, I.S., Brown, L., 2003. Seasonal

constraints on the estimation of new production from space using temperature-nitrate relationships. Geophys. Res. Lett. 30. https://doi.org/10.1029/2003gl017982.
van Heuven, S., Pierrot, D., Rae, J.W.B., Lewis, E., Wallace, D.W.R., 2011. CO2SYS v 1.1 MATLAB Program Developed for CO2 System Calculations. ORNL/CDIAC-105b.
Holte, J., Talley, L.D., Gilson, J., Roemmich, D., 2017. An Argo mixed layer climatology and database. Geophys. Res. Lett. 44, 5618–5626. https://doi.org/10.1002/2017GL073426.
Humphreys, M.P., Achterberg, E.P., Hopkins, J.E., Chowdhury, M.Z.H., Griffiths, A.M., Hartman, S.E., Hull, T., Smilenova, A., Wihsgott, J.U., Woodward, S., Malcolm, E., MarkMoorea, C., 2018. Mechanisms for a nutrient-conserving carbon pump in a seasonally stratified, temperate continental shelf sea. Prog. Oceanogr. https://doi.org/10.1016/j.pocean.2018.05.001.
Iida, Y., Kojima, A., Takatani, Y., Nakano, T., Sugimoto, H., Midorikawa, T., Ishii, M., 2015. Trends in pCO2 and sea–air CO2 flux over the global open oceans for the last two decades. J. Oceanogr. 71, 637–661. https://doi.org/10.1007/s10872-015-0306-4.
Jeansson, E., Bellerby, R.G.J., Skjelvan, I., Frigstad, H., Olafsdottir, S.R., Olafsson, J., 2015. Fluxes of carbon and nutrients to the Iceland Sea surface layer and inferred primary productivity and stoichiometry. Biogeosciences 12, 875–885. https://doi.org/10.5194/bg-12-875-2015.
Jiang, Z.P., Hydes, D.J., Tyrrell, T., Hartman, S.E., Hartman, M.C., Dumousseaud, C., Padin, X.A., Skjelvan, I., Gonzalez-Pola, C., 2013. Key controls on the seasonal and interannual variations of the carbonate system and air-sea CO2 flux in the Northeast Atlantic (Bay of Biscay). J. Geophys. Res. Oceans 118, 785–800. https://doi.org/10.1002/jgrc.20087.
Koeve, W., 2004. Spring bloom carbon to nitrogen ratio of net community production in the temperate N. Atlantic. Deep-Sea Res. Part I-Oceanogr. Res. Pap. 51, 1579–1600. https://doi.org/10.1016/j.dsr.2004.07.002.
Körtzinger, A., Send, U., Lampitt, R.S., Hartman, S., Wallace, D.W.R., Karstensen, J., Villagarcia, M.G., Llinas, O., DeGrandpre, M.D., 2008. The seasonal pCO(2) cycle at 49 degrees N/16.5 degrees W in the northeastern Atlantic Ocean and what it tells us about biological productivity. J. Geophys. Res. Oceans 113. https://doi.org/10.1029/2007jc004347.
Landschützer, P., Gruber, N., Bakker, D.C.E., Schuster, U., 2014. Recent variability of the global ocean carbon sink. Global Biogeochem. Cycles 28, 927–949. https://doi.org/10.1002/2014gb004853.
Landschützer, P., Gruber, N., Bakker, D.C.E., Schuster, U., Nakaoka, S., Payne, M.R., Sasse, T.P., Zeng, J., 2013. A neural network-based estimate of the seasonal to inter-annual variability of the atlantic ocean carbon sink. Biogeosciences 10, 7793–7815. https://doi.org/10.5194/bg-10-7793-2013.
Landschützer, P., Gruber, N., Bakker, D.C.E., Stemmler, I., Six, K.D., 2018. Strengthening seasonal marine CO2 variations due to increasing atmospheric CO2. Nat. Clim. Change 8, 146–150. https://doi.org/10.1038/s41558-017-0057-x.
Lauvset, S.K., Currie, K., Metzl, N., Shin-ichiro, N., Bakker, D.C.E., Sullivan, K., Sutton, A., O'Brien, K.M., Olsen, A., 2018. SOCAT Quality Control Cookbook -For SOCAT version 7-. available at: https://www.socat.info/index.php/publications-onsocat/.
Le Quéré, C., Andrew, R.M., Friedlingstein, P., Sitch, S., Hauck, J., Pongratz, J., Pickers, P.A., Korsbakken, J.I., Peters, G.P., Canadell, J.G., Arneth, A., Arora, V.K., Barbero, L., Bastos, A., Bopp, L., Chevallier, F., Chini, L.P., Ciais, P., Doney, S.C., Gkritzalis, T., Goll, D.S., Harris, I., Haverd, V., Hoffman, F.M., Hoppema, M., Houghton, R.A., Hurtt, G., Ilyina, T., Jain, A.K., Johannessen, T., Jones, C.D., Kato, E., Keeling, R.F., Goldewijk, K.K., Landschützer, P., Lefèvre, N., Lienert, S., Liu, Z., Lombardozzi, D., Metzl, N., Munro, D.R., Nabel, J.E.M.S., Nakaoka, S.I., Neill, C., Olsen, A., Ono, T., Patra, P., Peregon, A., Peters, W., Peylin, P., Pfeil, B., Pierrot, D., Poulter, B., Rehder, G., Resplandy, L., Robertson, E., Rocher, M., Rödenbeck, C., Schuster, U., Schwinger, J., Séférian, R., Skjelvan, I., Steinhoff, T., Sutton, A., Tans, P.P., Tian, H., Tilbrook, B., Tubiello, F.N., van der Laan-Luijkx, I.T., van der Werf, G.R., Viovy, N., Walker, A.P., Wiltshire, A.J., Wright, R., Zaehle, S., Zheng, B., 2018a. Global carbon budget 2018. Earth Syst. Sci. Data 10, 2141–2194. https://doi.org/10.5194/essd-10-2141-2018.
Le Quéré, C., Andrew, R.M., Friedlingstein, P., Sitch, S., Pongratz, J., Manning, A.C., Korsbakken, J.I., Peters, G.P., Canadell, J.G., Jackson, R.B., Boden, T.A., Tans, P.P., Andrews, O.D., Arora, V.K., Bakker, D.C.E., Barbero, L., Becker, M., Betts, R.A., Bopp, L., Chevallier, F., Chini, L.P., Ciais, P., Cosca, C.E., Cross, J., Currie, K., Gasser, T., Harris, I., Hauck, J., Haverd, V., Houghton, R.A., Hunt, C.W., Hurtt, G., Ilyina, T., Jain, A.K., Kato, E., Kautz, M., Keeling, R.F., Klein Goldewijk, K., Körtzinger, A., Landschützer, P., Lefèvre, N., Lenton, A., Lienert, S., Lima, I., Lombardozzi, D., Metzl, N., Millero, F., Monteiro, P.M.S., Munro, D.R., Nabel, J.E.M.S., Nakaoka, S.I., Nojiri, Y., Padin, X.A., Peregon, A., Pfeil, B., Pierrot, D., Poulter, B., Rehder, G., Reimer, J., Rödenbeck, C., Schwinger, J., Séférian, R., Skjelvan, I., Stocker, B.D., Tian, H., Tilbrook, B., Tubiello, F.N., van der Laan-Luijkx, I.T., van der Werf, G.R., van Heuven, S., Viovy, N., Vuichard, N., Walker, A.P., Watson, A.J., Wiltshire, A.J., Zaehle, S., Zhu, D., 2018b. Global carbon budget 2017. Earth Syst. Sci. Data 10, 405–448. https://doi.org/10.5194/essd-10-405-2018.
Le Quéré, C., Takahashi, T., Buitenhuis, E.T., Rodenbeck, C., Sutherland, S.C., 2010. Impact of climate change and variability on the global oceanic sink of CO2. Global Biogeochem. Cycles 24. https://doi.org/10.1029/2009gb003599.
Lee, K., Tong, L.T., Millero, F.J., Sabine, C.L., Dickson, A.G., Goyet, C., Park, G.H., Wanninkhof, R., Feely, R.A., Key, R.M., 2006. Global relationships of total alkalinity with salinity and temperature in surface waters of the world's oceans. Geophys. Res. Lett. 33. https://doi.org/10.1029/2006gl027207.
Lefèvre, N., Veleda, D., Araujo, M., Caniaux, G., 2016. Variability and trends of carbon parameters at a time series in the eastern tropical Atlantic. Tellus Ser. B-Chem. Phys. Meteorol. 68. https://doi.org/10.3402/tellusb.v68.30305.
Longhurst, A., 2006. Ecological Geography of the Sea. Ecol. Geog. of the Sea Ser, second ed. Academic Press, San Diego, Calif.
Lueker, T.J., Dickson, A.G., Keeling, C.D., 2000. Ocean pCO(2) calculated from dissolved inorganic carbon, alkalinity, and equations for K-1 and K-2: validation based on laboratory measurements of CO2 in gas and seawater at equilibrium. Mar. Chem. 70, 105–119. https://doi.org/10.1016/s0304-4203(00)00022-0.
McDougall, T.J., Barker, P.M., 2011. Getting started with TEOS-10 and the Gibbs Seawater (GSW). Oceanogr. Toolbox 127.
McKinley, G.A., Fay, A.R., Takahashi, T., Metzl, N., 2011. Convergence of atmospheric and North Atlantic carbon dioxide trends on multidecadal timescales. Nat. Geosci. 4, 606. https://doi.org/10.1038/ngeo1193.
McKinley, G.A., Pilcher, D.J., Fay, A.R., Lindsay, K., Long, M.C., Lovenduski, N.S., 2016. Timescales for detection of trends in the ocean carbon sink. Nature 530, 469. https://doi.org/10.1038/nature16958.
Metzl, N., Corbière, A., Reverdin, G., Lenton, A., Takahashi, T., Olsen, A., Johannessen, T., Pierrot, D., Wanninkhof, R., Ólafsdóttir, S.R., Olafsson, J., Ramonet, M., 2010. Recent acceleration of the sea surface fCO2 growth rate in the North Atlantic subpolar gyre (1993–2008) revealed by winter observations. Global Biogeochem. Cycles 24. https://doi.org/10.1029/2009GB003658.
Midorikawa, T., Ishii, M., Nemoto, K., Kamiya, H., Nakadate, A., Masuda, S., Matsueda, H., Nakano, T., Inoue, H.Y., 2006. Interannual variability of winter oceanic CO2 and air-sea CO2 flux in the western North Pacific for 2 decades. J. Geophys. Res. Oceans 111. https://doi.org/10.1029/2005jc003095.
Ocean Productivity, 2016. Net primary production standard products. URL https://www.science.oregonstate.edu/ocean.productivity/.
Olsen, A., Brown, K.R., Chierici, M., Johannessen, T., Neill, C., 2008. Sea-surface CO(2) fugacity in the subpolar North Atlantic. Biogeosciences 5, 535–547. https://doi.org/10.5194/bg-5-535-2008.
Olsen, A., Wanninkhof, R., Triñanes, J.A., Johannessen, T., 2005. The effect of wind speed products and wind speed—gas exchange relationships on interannual variability of the air—sea CO2 gas transfer velocity. Tellus B: Chem. Phys. Meteorol. 57, 95–106. https://doi.org/10.3402/tellusb.v57i2.16777.
Palevsky, H.I., Quay, P.D., 2017. Influence of biological carbon export on ocean carbon uptake over the annual cycle across the North Pacific Ocean. Global Biogeochem. Cycles 31, 81–95. https://doi.org/10.1002/2016gb005527.
Park, P.K., 1969. Oceanic CO2 system: an evaluation of ten methods of investigation. Limnol. Oceanogr. 14, 179–186. https://doi.org/10.4319/lo.1969.14.2.0179.
Pereira, R., Ashton, I., Sabbaghzadeh, B., Shutler, J.D., Upstill-Goddard, R.C., 2018. Reduced air–sea CO2 exchange in the Atlantic Ocean due to biological surfactants. Nat. Geosci. 11, 492–496. https://doi.org/10.1038/s41561-018-0136-2.
Pierrot, D., Neill, C., Sullivan, K., Castle, R., Wanninkhof, R., Luger, H., Johannessen, T., Olsen, A., Feely, R.A., Cosca, C.E., 2009. Recommendations for autonomous underway pCO(2) measuring systems and data-reduction routines. Deep-Sea Res. Part II-Top. Stud. Oceanogr. 56, 512–522. https://doi.org/10.1016/j.dsr2.2008.12.005.
Rödenbeck, C., Bakker, D.C.E., Gruber, N., Iida, Y., Jacobson, A.R., Jones, S., Landschützer, P., Metzl, N., Nakaoka, S., Olsen, A., Park, G.H., Peylin, P., Rodgers, K.B., Sasse, T.P., Schuster, U., Shutler, J.D., Valsala, V., Wanninkhof, R., Zeng, J., 2015. Data-based estimates of the ocean carbon sink variability – first results of the Surface Ocean pCO2 Mapping intercomparison (SOCOM). Biogeosciences 12, 7251–7278. https://doi.org/10.5194/bg-12-7251-2015.
Robson, J., Ortega, P., Sutton, R., 2016. A reversal of climatic trends in the North Atlantic since 2005. Nat. Geosci. 9, 513–517. https://doi.org/10.1038/ngeo2727.
Sabine, C.L., Feely, R.A., Gruber, N., Key, R.M., Lee, K., Bullister, J.L., Wanninkhof, R., Wong, C.S., Wallace, D.W.R., Tilbrook, B., Millero, F.J., Peng, T.H., Kozyr, A., Ono, T., Rios, A.F., 2004. The oceanic sink for anthropogenic CO2. Science 305, 367–371. https://doi.org/10.1126/science.1097403.
Sambrotto, R.N., Savidge, G., Robinson, C., Boyd, P., Takahashi, T., Karl, D.M., Langdon, C., Chipman, D., Marra, J., Codispoti, L., 1993. Elevated consumption of carbon relative to nitrogen in the surface ocean. Nature 363, 248. https://doi.org/10.1038/363248a0.
Schlitzer, R., 2016. Ocean data view. URL http://odv.awi.de.
Schuster, U., Watson, A.J., 2007. A variable and decreasing sink for atmospheric CO2 in the North Atlantic. J. Geophys. Res. Oceans 112. https://doi.org/10.1029/2006jc003941.
Schuster, U., Watson, A.J., Bates, N.R., Corbiere, A., Gonzalez-Davila, M., Metzl, N., Pierrot, D., Santana-Casiano, M., 2009. Trends in North Atlantic sea-surface fCO2 from 1990 to 2006. Deep Sea Res. Part II: Top. Stud. Oceanogr. 56, 620–629. https://doi.org/10.1016/j.dsr2.2008.12.011.
Seki, O., Foster, G.L., Schmidt, D.N., Mackensen, A., Kawamura, K., Pancost, R.D., 2010. Alkenone and boron-based Pliocene pCO2 records. Earth Planet. Sci. Lett. 292, 201–211. https://doi.org/10.1016/j.epsl.2010.01.037.
Shadwick, E.H., Thomas, H., Azetsu-Scott, K., Greenan, B.J.W., Head, E., Horne, E., 2011. Seasonal variability of dissolved inorganic carbon and surface water pCO(2) in the Scotian Shelf region of the Northwestern Atlantic. Mar. Chem. 124, 23–37. https://doi.org/10.1016/j.marchem.2010.11.004.
Shutler, J.D., Land, P.E., Brown, C.W., Findlay, H.S., Donlon, C.J., Medland, M., Snooke, R., Blackford, J.C., 2013. Coccolithophore surface distributions in the North Atlantic and their modulation of the air-sea flux of CO2 from 10 years of satellite Earth observation data. Biogeosciences 10, 2699–2709. https://doi.org/10.5194/bg-10-2699-2013.
Steinberg, D.K., Carlson, C.A., Bates, N.R., Johnson, R.J., Michaels, A.F., Knap, A.H., 2001. Overview of the US JGOFS Bermuda Atlantic Time-series Study (BATS): a decade-scale look at ocean biology and biogeochemistry. Deep-Sea Res. Part II-Top. Stud. Oceanogr. 48, 1405–1447. https://doi.org/10.1016/s0967-0645(00)00148-x.
Takahashi, T., Olafsson, J., Goddard, J.G., Chipman, D.W., Sutherland, S.C., 1993. Seasonal variation of CO2 and nutrients in the high-latitude surface oceans: a comparative study. Global Biogeochem. Cycles 7, 843–878. https://doi.org/10.1029/93GB02263.
Takahashi, T., Sutherland, S.C., Sweeney, C., Poisson, A., Metzl, N., Tilbrook, B., Bates,

N., Wanninkhof, R., Feely, R.A., Sabine, C., Olafsson, J., Nojiri, Y., 2002. Global sea–air CO2 flux based on climatological surface ocean pCO2, and seasonal biological and temperature effects. Deep Sea Res. Part II: Top. Stud. Oceanogr. 49, 1601–1622. https://doi.org/10.1016/S0967-0645(02)00003-6.

Takahashi, T., Sutherland, S.C., Wanninkhof, R., Sweeney, C., Feely, R.A., Chipman, D.W., Hales, B., Friederich, G., Chavez, F., Sabine, C., Watson, A., Bakker, D.C.E., Schuster, U., Metzl, N., Yoshikawa-Inoue, H., Ishii, M., Midorikawa, T., Nojiri, Y., Körtzinger, A., Steinhoff, T., Hoppema, M., Olafsson, J., Arnarson, T.S., Tilbrook, B., Johannessen, T., Olsen, A., Bellerby, R., Wong, C.S., Delille, B., Bates, N.R., de Baar, H.J.W., 2009. Climatological mean and decadal change in surface ocean pCO2, and net sea–air CO2 flux over the global oceans. Deep Sea Res. Part II: Top. Stud. Oceanogr. 56, 554–577. https://doi.org/10.1016/j.dsr2.2008.12.009.

Tesdal, J.E., Abernathey, R.P., Goes, J.I., Gordon, A.L., Haine, T.W.N., 2018. Salinity trends within the upper layers of the Subpolar North Atlantic. J. Clim. 31, 2675–2698. https://doi.org/10.1175/JCLI-D-17-0532.1.

Tjiputra, J.F., Olsen, A., Bopp, L., Lenton, A., Pfeil, B., Roy, T., Segschneider, J., Totterdell, I.J., Heinze, C., 2014. Long-term surface pCO2 trends from observations and models. Tellus B: Chem. Phys. Meteorol. 66, 23083. https://doi.org/10.3402/tellusb.v66.23083.

Toggweiler, J.R., 1993. Oceanography - Carbon Overconsumption. Nature 363, 210–211. https://doi.org/10.1038/363210a0.

Wanninkhof, R., 2014. Relationship between wind speed and gas exchange over the ocean revisited. Limnol. Oceanogr. Methods 12, 351–362. https://doi.org/10.4319/lom.2014.12.351.

Wanninkhof, R., Park, G.H., Takahashi, T., Sweeney, C., Feely, R., Nojiri, Y., Gruber, N., Doney, S.C., McKinley, G.A., Lenton, A., Le Quere, C., Heinze, C., Schwinger, J., Graven, H., Khatiwala, S., 2013. Global ocean carbon uptake: magnitude, variability and trends. Biogeosciences 10, 1983–2000. https://doi.org/10.5194/bg-10-1983-2013.

Wanninkhof, R., Triñanes, J., 2017. The impact of changing wind speeds on gas transfer and its effect on global air-sea CO2 fluxes. Global Biogeochem. Cycles 31, 961–974. https://doi.org/10.1002/2016GB005592.

WDCGG, 2018. Mace Head xCO2. URL https://gaw.kishou.go.jp/.

Weiss, R., 1974. Carbon dioxide in water and seawater: the solubility of a non-ideal gas. Mar. Chem. 2, 203–215.

Wolf-Gladrow, D.A., Zeebe, R.E., Klaas, C., Körtzinger, A., Dickson, A.G., 2007. Total alkalinity: The explicit conservative expression and its application to biogeochemical processes. Mar. Chem. 106, 287–300. https://doi.org/10.1016/j.marchem.2007.01.006.

Wong, C.S., Waser, N.A.D., Nojiri, Y., Johnson, W.K., Whitney, F.A., Page, J.S.C., Zeng, J., 2002. Seasonal and interannual variability in the distribution of surface nutrients and dissolved inorganic carbon in the northern North Pacific: Influence of El Nino. J. Oceanogr. 58, 227–243. https://doi.org/10.1023/a:1015897323653.

Zunino, P., Lherminier, P., Mercier, H., Padin, X.A., Rios, A.F., Perez, F.F., 2015. Dissolved inorganic carbon budgets in the eastern subpolar North Atlantic in the 2000s from in situ data. Geophys. Res. Lett. 42, 9853–9861. https://doi.org/10.1002/2015gl066243.